Distribution of Magnetic Field Components in the Solar Wind Plasma

N. S. Padhye, C. W. Smith, and W. H. Matthaeus

Bartol Research Institute, University of Delaware, Newark, DE 19716

Short title: DISTRIBUTION OF MAGNETIC FIELD IN THE SOLAR WIND

February 12, 2001

Abstract.

We examine the probability distribution functions (PDF's) of fluctuations of magnetic field components using the Ulysses and Omnitape datasets to evaluate departures from Gaussian distributions. Functional fits as well as moment comparisons (kurtoses) are used in drawing conclusions concerning the degree of non-Gaussianity. Short-time-scale fluctuations are separated, to the extent possible, from the longer-time-scale variation of the mean field, and attention is paid to data selection issues such as stationarity. At the present level of comparison, it seems that departures from Gaussianity of the distributions of the fluctuations are not severe. The analysis is carried out in the mean field coordinates in which the fluctuations of components are close to being uncorrelated, and it is observed that the perpendicular components are closer to being Gaussian than the parallel one. It is shown that the kurtosis is highly exaggerated when the variation of the mean field is not taken into account. We further examine the distributions of hourly magnetic field fluctuations in fast and slow solar wind at different phases in the solar cycle in order to quantitatively describe departures from the Gaussian distribution. It is found that the kurtosis lies between 2.8 and 4.8 for all components in the mean field coordinates, in both fast and slow wind and near solar maximum and near solar minimum. It appears that the distributions of fluctuations are rather more similar with regard to their degree of non-Gaussianity than might have been expected based upon the well documented differences in the characteristics of fast and slow solar wind intervals. This suggests a robust form of statistical similarity that may be associated with either *in situ* or source region nonlinear effects. In addition to the

distributions of the fluctuations, we present the distributions of the mean field and of the variances of the components which are more likely to be influenced by solar sources than by interplanetary dynamical processes. The PDF's of variances of the magnetic field components over different subintervals approximate lognormal curves, and provide the motivation to compute the PDF's of the fluctuations using the approach of *Castaing et al.* [1990], which is a superposition of Gaussian distributions with variances that are distributed lognormally. The resulting PDF's of the fluctuations provide a good model to describe the small departures from Gaussian distributions seen in the observed PDF's. An additional step is taken to compute the expected PDF of the magnitude of the fluctuations from the Castaing PDF's of the components, and is also seen to be in good agreement with the observed PDF.

1. Introduction

The probability distribution function (PDF) describes the relative frequency of occurrence of magnetic fluctuations ($\mathbf{b}$) in a turbulent medium such as the solar wind. It is of comparable importance in solar wind research to the role of the PDF of velocity fluctuations in turbulent hydrodynamics [see, e.g. *Monin and Yaglom*, 1975] to the degree that in the solar wind both the velocity and magnetic fluctuations are reasonably well described by magnetohydrodynamics (MHD). The PDF of $\mathbf{b}(\mathbf{x}, t)$ (spatial $\mathbf{x}$ and time t coordinates) is of fundamental importance in any statistical description of the fluctuations, whether it be kinematic or dynamical. Therefore it is essential to provide for it a firm observational basis, which is the principal goal of the present paper. Of particular importance is the degree of departure of the PDF from the Gaussian or normal distribution, which is a reference distribution for a variety of reasons. The fluctuations are normally distributed if the PDF's of the components are:

$$P_i(b_i) = \frac{1}{\sqrt{2\pi}\,\sigma_i} \exp\left(-\frac{b_i^2}{2\,\sigma_i^2}\right) , \qquad i = 1, 2, 3 , \tag{1}$$

where $\sigma_i^2 = \langle b_i^2 \rangle$ is the variance and the angular brackets denote ensemble averaging. As a baseline for many further and more sophisticated statistical studies, one would like to have an observational consensus regarding the quantitative degree to which the distributions depart from Gaussian. Unfortunately such a consensus does not appear in the published literature, and there are widely disparate reports of the degree of "non-Gaussianity" [*Whang*, 1977; *Feynman and Ruzmaikin*, 1994]. Clarification of this observational issue is one of our motivations for the present paper.

There are also important motivations that arise from a theoretical perspective. For example, it is well known in homogeneous hydrodynamic turbulence theory that nonlinearities vanish when the triple correlations (third moments of the PDF) vanish [e.g., *Lesieur*, 1990; *Monin and Yaglom*, 1975]. A similar feature is obtained for incompressible MHD turbulence [*Grappin et al.*, 1982]. Since triple correlations vanish for a Gaussian field, it is clear that non-Gaussianity is required for nonlinearity. Therefore, for incompressible and nearly incompressible [*Zank and Matthaeus*, 1993] turbulence the degree of non-Gaussianity is a measure of nonlinearity and turbulent activity.

A related issue is that of "quasinormality." The quasinormal hypothesis, also known as the *Millionshchikov* [1941] hypothesis [see also, *Heisenberg*, 1948; *Monin and Yaglom*, 1975], is the approximation that the value of fourth order moments take on their Gaussian values, while the third order moments are permitted to depart from their Gaussian value of zero. Clearly, distributions for which this hypothesis is valid need not be precisely Gaussian but may exhibit distinctive but small non-Gaussian features. One particularly important application of Millionshchikov's hypothesis is in dynamical closures such as the eddy-damped quasinormal Markovian model ["EDQNMA," see, e.g., *Orszag*, 1970; *Monin and Yaglom*, 1975] in which the quasi-normal approximation is invoked to derive a dynamical equation for the third order moments. An EDQNMA has been developed and solved numerically for MHD in a solar wind context [e.g., *Grappin et al.*, 1983]. Other applications of the quasinormal approximation include its use to evaluate pressure spectra in hydrodynamics [*Batchelor*, 1982] and weakly compressible

MHD density spectra [*Montgomery et al.*, 1987]. The latter theory was offered as an explanation for observed "Kolmogoroff-like" density spectra observed in the solar wind [*Goldstein and Siscoe*, 1972] and in the interstellar medium [*Armstrong et al.*, 1980]. The quasinormal approach has many applications in turbulence, a large number of which may not yet have been exploited fully in solar wind research. A better empirical understanding of the conditions for applicability of the quasinormal approximation in the solar wind would help to clarify and possibly motivate further applications of this type. This requires a statistically defensible baseline calculation of the degree of non-Gaussianity of the magnetic field fluctuations, which is the goal of this paper.

In one of the earliest works on probability distribution functions (PDF's) of fluctuations of interplanetary magnetic field components, *Whang* [1977] concludes that the fluctuations were Gaussian to a good approximation, but does not provide a quantitative measure of the departures from Gaussianity. Since then a number of authors have written about the non-Gaussianity of the PDF's, but we note that there is neither uniformity in the various analyses nor do they all refer to PDF's of the same physical quantity. *Whang* [1977] studies the components in the principal axes of anisotropy of the fluctuations of the magnetic field over short time periods (6 hours). *Feynman and Ruzmaikin* [1994] carry out their analysis using hourly averaged data over one year. They present the PDF's of the magnitude of the field and of one of the perpendicular components in the GSE coordinates, and do not attempt to separate the fluctuations from the variations of the mean field. They conclude that the two PDF's are neither Gaussian nor lognormal, and provide a quantitative measure of the

departures from Gaussianity.

Marsch and Tu [1994] present the PDF's of *increments* (at various lags) of the magnetic field components in the RTN coordinate frame. Their data set spans approximately eight days, and they find that the PDF's are progressively more Gaussian at larger values of the lag. Computation of increments eliminates dependence upon the mean field in the data set, but only in the case of a constant mean field. *Kabin and Papitashvili* [1998] present the PDF's of increments (at short lags) of one of the components in the RTN frame. *Sorriso–Valvo et al.* [1999] and *Bruno et al.* [1999] compute PDF's of the *normalized increments* (the standard deviation on subintervals is normalized to unity before the data from different subintervals is combined) of the magnitude and of one of the components of the magnetic field in the RTN coordinate frame. *Burlaga* [1991b] studies only the PDF of the magnitude of the magnetic field, and not of the vector components.

We should remark at this point that many of the above studies are oriented towards study of small scale "intermittency" which is signified by non-Gaussian values of higher order moments [*Monin and Yaglom*, 1975], and in particular the increase of this effect for data computed with smaller increment lags. This signifies important features of the derivatives of the turbulent field $\mathbf{b}$, in contrast to the primitive turbulent field itself. It is however very much outside the scope of the present study, which focuses exclusively on the PDF of the primitive field $\mathbf{b}$, and which is motivated quite differently, as we emphasized in our opening paragraphs above.

A quantitative measure of departure from the Gaussian distribution is provided

by the kurtosis of a random variable $\Omega = \langle\Omega\rangle + \omega$, defined as $\kappa = \langle\omega^4\rangle/\langle\omega^2\rangle^2$. For a Gaussian distribution all odd central moments vanish, $\langle\omega^{(2m+1)}\rangle = 0$, $m = 1, 2, \ldots$, while all even central moments are determined by the variance $\langle\omega^2\rangle$. The kurtosis has a value $\kappa = 3$ for a scalar random variable or a component of a vector having a Gaussian distribution. Suppose a signal with zero mean consists of fixed intensity pulses with fixed duration that occur at random times and with random signs, and that the fraction of time in which the pulses are "on" is f. Then one can easily see that the kurtosis is $\kappa = 1/f$. Thus the kurtosis behaves like the reciprocal of the "filling factor" for the signal.

When a random field displays a nonuniform or bursty character in either space or time, it can be said to be "intermittent". This corresponds to a small filling factor f, and a large kurtosis compared with nonbursty signals. Typically, intermittency is associated with an elevated probability of large values, and a concomitant decrease in the occurrence of small values. Highly intermittent signals necessarily have a non-Gaussian distribution [*Monin and Yaglom*, 1975, vol. 2, p. 241 and 271]. In recent years the emphasis in intermittency studies has been placed on the progressively greater non-Gaussianity that is seen at small scales, and in particular the greater non-Gaussianity displayed by the spatial derivative of the primitive turbulent random field. Small scale intermittency and intermittency of dissipation is a topic of great interest in hydrodynamics [*She and Leveque,* 1994; *Wang et al.,* 1999] and in magnetohydrodyamics (MHD) [*Politano and Pouquet,* 1995] and space plasma physics as well [*Burlaga,* 1991a, *Marsch and Tu,* 1994, *Marsch et al.,* 1996, *Bruno et al.,* 1999,

e. g.], and the departures from Gaussian distributions are described frequently by study of the scaling of higher order moments. The beta model [*Frisch et al.,* 1978] and multifractal representations [*Burlaga,* 1991b; *Kabin and Papitashvili,* 1998] are familiar examples.

Here we are interested solely in the question of the non-Gaussianity of the turbulent magnetic field itself, not its derivatives, or the spatial distribution of dissipation. We present PDF's that arise from a new analysis of data that is distinct from the previous analyses. We view the PDF of the magnetic field in the solar wind plasma as the superposition of the PDF of the mean field, presumably a property of the solar source, and the PDF of fluctuations relative to the mean field. Operationally, the fluctuations are on a short time-scale, while the mean field varies on a longer time-scale. Data analysis carried out from this perspective leads to the conclusion that the deviation of the PDF's of the fluctuations of the magnetic field components from Gaussian distributions is not as significant as it may seem when the mean field variation is not taken into account [*Feynman and Ruzmaikin*, 1994; *Ruzmaikin et al.*, 1995]. Our analysis is most directly comparable to that of *Whang* [1977] and *Feynman and Ruzmaikin* [1994], and reconciles the opposing conclusions of the two works. We base our judgement on quantitative measures of departures from Gaussianity provided by the kurtoses κ and the goodness-of-fit parameter χ^2. Note that while it is plausible that our conclusions may be comparable to those of the works on PDF's of increments [e. g. *Marsch and Tu*, 1994] at long lags (1 hr or longer), the precise relationship of PDF's of fluctuations from the mean field to those of increments is not clear. For very

short lags, the PDF of increments of a field approach the PDF of its derivative, while at very long lags (longer than typical correlation times of about 6 to 12 hours in the solar wind), the PDF of increments of a field approach the PDF of the field itself.

It has been shown [*Hartlep et al.*, 2000] that if the components of a vector have Gaussian distributions, and are independent, the PDF of the magnitude of the vector appoximates the lognormal distribution often used to characterize the PDF of magnetic field magnitudes [*Burlaga and King*, 1979; *Slavin and Smith*, 1983; *Burlaga and Ness*, 1998]. Here, we focus our attention mainly on the PDF's of the components of the magnetic field fluctuations, and of the separate PDF's of the underlying mean field and variances of the components. In addition to comparison of the PDF's of the components and their kurtoses to Gaussian distributions, we also compare them to Castaing distributions, which are introduced in Sec. 2 and further explored in Sec. 4. Following *Hartlep et al.* [2000], the PDF of the fluctuation magnitude is derived from the distributions of components as expected from the Castaing model, and is compared to the observed distribution of the fluctuation magnitude.

2. Methodology and Overview

Examination of the PDF's of magnetic field fluctuations in the solar wind plasma necessitates the removal of the mean field from spacecraft measurements. Estimation of the mean field is an important issue that is complicated by the presence of fluctuation power at very low frequencies associated with solar source processes [e. g. *Matthaeus and Goldstein*, 1986] and by the existence of adjacent time intervals with different statistical

properties. This is most evident during events such as magnetic clouds and current sheet crossings, but is not restricted to these events alone. We use a stationarity test of the mean, described briefly in Sec. 3.1, which attempts to detect and eliminate intervals with multiple statistical means. This is not a central feature of our analysis since its absence does not change the conclusions to a significant extent, but we employ the test since it is an important conceptual component.

We analyze hourly averaged magnetic field data from the NSSDC Omnitape over a span of 30 years, and 1 minute magnetic field averages from Ulysses over a period of 2 months. In order to extract the variation of the mean magnetic field, we break the data into smaller intervals. This interval needs to be small so that variations in the mean field can be tracked as accurately as possible, but it has to be long enough to measure the mean field to good accuracy. (The statistical error in the determination of the mean field is determined by the ratio of the interval length to the correlation time of the fluctuations and is presented in Sec. 3.1.) Empirically we have found that an interval length of about four days works well, but the analysis is clearly not independent of this choice, so we present an analysis of the Ulysses data using 4-day intervals and repeat the analysis using 1-day intervals to illustrate differences in the resulting PDF's.

Computation of the mean field on an individual interval allows us to transform to the mean field coordinate system in which the magnetic field may be expressed as

$$\mathbf{B} = b_1\,\mathbf{e}_{\perp 1} + b_2\,\mathbf{e}_{\perp 2} + (B_0 + b_3)\,\mathbf{e}_{\parallel}\,, \tag{2}$$

where B_0 is the mean field, and b_1, b_2, and b_3 are the orthogonal fluctuations. The

direction $\mathbf{e}_{\parallel}$ is evidently that of the mean field, while the choices of the other two directions $\mathbf{e}_{\perp 1}$ and $\mathbf{e}_{\perp 2}$ are explained in Sec. 3. Note that B_0 is defined uniquely on each interval in the data analysis algorithm, but it varies both in time and in space. In the simplest idealization we would like to associate B_0 with a sharply defined ensemble average mean field suggested by Eq. (2). However, variability of the local mean due to solar source variations along with finite sampling errors (see Sec. 3.1) will influence statistics based upon our empirically determined decomposition. The use of increments [e. g. *Marsch and Tu*, 1994] improves the statistics [*Panchev*, 1971] in some cases, but does not remove errors due to spatial variation of the mean field.

We have found that the fluctuations of the three components are very nearly uncorrelated in the mean field coordinate frame, which is a strong motivating factor to perform the analysis in this reference frame. The evidence for the statistical uncorrelatedness of the fluctuations is provided by the cross-correlation matrix $\langle b_i\, b_j \rangle$, and is presented in Sec. 3. Furthermore, the mean field provides a direction of basic anisotropy [*Matthaeus and Smith*, 1981] that reflects in situ dynamics, so it is the logical coordinate system to use from that point of view as well.

The mean field itself is not constant in time, therefore we present the PDF's of the mean magnetic field and of the variances of the components. These distributions provide a measure of the variability and uncertainty in the parameters that characterize the component distributions.

The importance of separating the short-time-scale fluctuations from the long-time-scale variation of the mean field is presented in Sec. 3.2, where it is shown by means of

an example that the kurtosis of a component distribution can drop dramatically upon removing the variations of the mean field.

In Sec. 3.3 we address the differences between PDF's of the fast and slow wind. It has been known since the early exploration of the interplanetary medium that intervals of solar wind observations in the ecliptic could be meaningfully separated into periods with radial solar wind speeds $U \lesssim 500$ km/s and fast wind periods with $U \gtrsim 500$ km/s. The Ulysses mission has confirmed that the dichotomy of fast and slow wind is explained principally as spatial organization of the wind sources. Fast wind generally originates at higher latitudes from coronal hole regions while slow wind generally emerges from lower latitude streamer belt regions. A strong source of temporal variation is the 11 year solar cycle which alternately expands the influence of slow and fast wind in the heliospheric volume, so that at solar minimum a fairly steady fast wind with $U > 600$ km/s occupies most of the volume except within perhaps $\pm 20^\circ$ of the heliographic equator. The contrast in gross properties of the slow and fast wind is fairly striking, the fast wind being hotter and less dense [*Hundhausen,* 1972; *Phillips et al.,* 1995]. There are also observed differences in minor ion species composition, proton anisotropies, electron beams, Coulomb collisionality, and other properties [*Feldman and Marsch,* 1997]. It is not surprising that magnetic field and plasma fluctuations also exhibit clear differences. Indeed fluctuations in the fast wind are relatively steadier and more Alfvénic than their slow wind counterparts [*Goldstein et al.,* 1995; *Tu and Marsch,* 1995].

In view of these extensive differences, one might expect that the probability distribution of fluctuations in the fast and slow wind would differ substantially, however

this appears to be an incompletely settled issue at present. Comparisons between any two works on the subject are not clear due to the diversity of procedures used by authors in their analyses. Some authors have argued that the slow wind is more non-Gaussian than the fast wind [*Marsch and Tu,* 1994], particularly so on time scales of several hours, while others [*Smith and Balogh,* 1995; *Sorriso-Valvo et al.,* 1999] have suggested that fast and slow wind distributions are very similar. In Sec. 3.3 we attempt to provide a clear characterization of the degree of non-Gaussianity of MHD scale fluctuations in the fast and slow wind using hourly averaged spacecraft data. We present evidence that the fast and slow wind distributions are quite similar, and have almost the same degree of non-Gaussian character, as measured by the kurtoses of the distributions.

In Sec. 4 we present a model that can reproduce the small departures from Gaussianity seen in the distributions of fluctuations. The observed fluctuations, particularly of the parallel component, show small, but persistent, departures from Gaussian distributions. Furthermore, the PDF's of variances of the components are approximately lognormal, suggesting that the superposition approach of *Castaing et al.* [1990] may be appropriate to model the PDF's of the IMF fluctuations. Stated simply, the Castaing model is a superposition of Gaussian distributions with variances that are distributed lognormally. Such a model is physically plausible since it is well known that the IMF at low latitudes arises from many discrete coronal sources. If the conjecture is then made that each of these discrete sources gives rise to Gaussianly distributed magnetic field components, it follows from the multiplicity of the sources that one may expect a spread of variances in the net magnetic field fluctuations. The distribution

of the variances may be considered a property of the sources and is a measure of the relative numbers of sources that give rise to magnetic field fluctuations with specific values of the variance. Effects of distributions of other physical properties over the collection of discrete sources have been studied by some authors [e. g. *Matthaeus and Goldstein*, 1986; *Mullan*, 1990].

The Castaing approach does seem to model the observed distributions well, and yields kurtoses and higher order even moments which are similar to those observed. Note that the Castaing model, being a superposition of Gaussians, has vanishing odd moments and is only proposed as a model for the higher order even moments. Only if a distribution of mean fields were included as well, would a Castaing approach admit non-zero odd moments. If a quasinormal analysis is desired, it would be necessary to determine the third moments from the higher order even moments and then set the higher order moments to their Gaussian values while allowing non-vanishing third moments. Curiously, the Castaing model seems to yield best results for two of the components, while one component is remarkably Gaussian.

When fluctuations of the components are statistically independent, the PDF of the magnitude of the fluctuations can be computed from those of the components, as discussed in Sec. 4.2. We derive the PDF of the fluctuation magnitude from the Castaing-superposed PDF's of the component fluctuations. The resulting PDF is seen to be in close agreement with the observations.

Castaing superposition has been used in the context of PDF's of the IMF by *Sorriso-Valvo et al.* [1999], where the authors address the inverse problem of determining

the width of the lognormal distribution of the variance from the PDF of *increments* of the magnitude of the magnetic field. Our use of the Castaing model has three notable differences. First, we are concerned with the PDF's of the fluctuations, not those of the time-lagged increments. Second, we apply the model to individual components, and not to the magnitude. We derive the PDF of the magnitude from those of the components. Third, we do not address the inverse problem, but use the best-fit lognormal to the observed PDF's of variances of the components to calculate the Castaing-superposed PDF's.

3. Observed Distributions of Magnetic Field Components

The magnetic field data that we analyze here is from the NSSDC Omnitape [*King and Papitashvili*, 1994] and Ulysses spacecraft [*Balogh et al.*, 1992]. The Omnitape near-Earth data consists of 1 hour magnetic field averages over a 30 year span from 1965 through 1994, while the Ulysses data consists of 1 minute magnetic field averages during the first two months of 1991. Note that the relatively short period of the Ulysses data was necessitated by the rapid movement of the spacecraft away from the Sun and towards Jupiter in the plane of the ecliptic during 1991. During the first two months of 1991 Ulysses moved from 1.59 AU to 2.24 AU from the Sun, a radial distance of 0.65 AU in the ecliptic [*Smith and Marsden*, 1995].

In the analyses of Omnitape and Ulysses data, we calculate mean fields over time intervals of 96 hour duration, and also repeat the analysis of Ulysses data on 24 hour averaging intervals for the sake of comparison. We have carried out the analyses using

various lengths of the averaging interval for both data sets, and found that 96 hour averaging intervals work well since they are long enough to determine the mean field to reasonable accuracy, and short enough that there is good likelihood that the averaging interval is not composed of two or more patches with statistical properties different from one another. The 96 hour interval also has the advantage of being sufficiently longer than typical correlation times in the solar wind plasma, yet much shorter than the solar rotation period.

Spacecraft data often has fill values representing missing (gaps) or corrupted (bad) measurements, and we only accept those intervals that have less than 25% fill values. In the case of the Omnitape data this leads to the elimination of close to 60% of the available data, while the loss of data is under 3% in the case of Ulysses. The high fraction of elimination of the Omnitape composite data is due to unavailability of data during many time spans.

After computing the mean field on each 96 hour interval, we transform to the mean field coordinate system [*Belcher and Davis*, 1971]. In this reference frame fluctuations are specified by the two perpendicular components and one parallel component that has the mean field subtracted out. The "second" perpendicular direction is defined by

$$\mathbf{e}_{\perp 2} := \frac{\mathbf{e}_{\parallel} \times \mathbf{e}_r}{|\mathbf{e}_{\parallel} \times \mathbf{e}_r|} ,$$

where $\mathbf{e}_{\parallel}$ is the direction along the mean field and $\mathbf{e}_r$ is the radial direction away from the Sun. The "first" perpendicular direction $\mathbf{e}_{\perp 1} := \mathbf{e}_{\perp 2} \times \mathbf{e}_{\parallel}$ is uniquely determined so that the resulting coordinate system is right handed.

The mean field coordinate system is well suited to the analysis since the components are very nearly statistically uncorrelated in this frame. The cross-correlation matrix $\langle b_i\, b_j \rangle$ is symmetric, and the off-diagonal elements can be compared to the diagonal elements to measure the significance of the cross-correlation. In particular the normalized cross-correlation between components b_1 and b_2 can be measured by $< b_1\, b_2 > / \sqrt{< b_1^2 >< b_2^2 >}$. For the one analysis with Omnitape, and two with Ulysses that are presented here, we have found the normalized cross-correlation between components 1 and 2 (the two perpendicular components) to be 0.3%, 5.0%, and 2.4% respectively. In the case of components 2 and 3 we obtain 3.0%, 2.4%, and 1.8%, while for components 3 and 1 we get 2.0%, 9.0%, and 4.8%.

Note also that since a symmetric matrix can always be diagonalized, it is guaranteed that there exists a reference frame in which the fluctuations are statistically uncorrelated. Test calculations that we performed in this frame (in which the fluctuations are uncorrelated by construction) indicate that the PDF's are very nearly identical to the ones obtained in the mean field reference frame. For this reason, and since the mean field frame is more intuitive, we have decided to carry out the analyses in this reference frame.

A data selection criterion that we employ at this stage of the analysis is a stationarity test of the mean [*Matthaeus, Goldstein, and King*, 1986] which can detect and eliminate intervals that are composed of patches with two or more different means. Examples of such intervals are magnetic cloud and current sheet crossings, but the stationarity test is additionally capable of detecting subtler changes of mean. The

criterion used by the test is explained briefly in the next section, and its use leads to the elimination of approximately 60% of the data that passes the fill-value test. It is also important to note that all of the analysis presented here has been repeated without using the stationarity test as a data selection criterion. The results with and without the stationarity test of the mean are similar, and do not lead to fundamentally different conclusions. We employ this test because theories of statistical analyses [e. g. *Panchev*, 1971] are usually applicable to stationary situations, and we wish to ensure, as much as possible, that the intervals we analyze are representative of a stationary ensemble.

The data from all available intervals is distributed into 50 bins of variable width such that each bin has an equal number of data points, m. This ensures equal statistical weight for each point of the PDF. The probability distribution function is defined by

$$f(b_i) = \frac{1}{N}\frac{m}{\Delta b_i}\,, \tag{3}$$

where Δb_i is the bin-width of the ith bin, and b_i is its center. The normalization factor $1/N$ ensures that the sum of probabilities adds up to one: $\int f(b)\,db = 1$, where the integration is over the range of observed values of b. The arithmetic mean of all the measurements contained in a bin is defined to be the center of the bin b_i.

The uncertainty in the computation of the center of the bin is given by $\sigma_i/\sqrt{m}$, where σ_i is the standard deviation of the points in the ith bin [*Bevington*, 1969]. For data from either spacecraft, the uncertainty is typically less than 0.5% for the component PDF's, which is true for bins that are near the peak of the PDF's as well as those on the tails. The uncertainty is too small to be shown in the plots of component PDF's.

The first set of plots shown in Fig. 1 are obtained from the hourly averaged Omnitape data. The analysis is carried out on intervals of 96 hour duration, and intervals are checked for stationarity prior to being included in the analysis. The solid curve is the best-fit Gaussian as computed from the least-squares method. The goodness-of-fit is measured by χ^2, which is defined as

Fig. 1

$$\chi^2 := \frac{\Sigma_i \left(f_1(b_i) - f_2(b_i)\right)^2 \, \Delta b_i}{\Sigma_i f_1^2(b_i) \, \Delta b_i} \,, \tag{4}$$

where $f_1(b_i)$ is the observed PDF and $f_2(b_i)$ is a Gaussian distribution. The least-squares method minimizes χ^2 to find the best-fit Gaussian. The values of the parameter χ^2 for the best-fit Gaussian are listed for each component in Table 1.

Table 1

Due care has been taken to ensure that each observed PDF and the adjoining Gaussian curves are normalized so that the area enclosed under each curve or observed PDF is equal to 1 *in the domain of observation.* This condition determines the amplitude of each Gaussian curve as a function of the mean b_0, variance σ^2, and end points of the domain. Thus the probability distribution function for an individual component b with mean b_0 is expressed as

$$f(b) = A \, \exp\left(-\frac{(b-b_0)^2}{2\,\sigma^2}\right) \,, \tag{5}$$

with the amplitude given by

$$A^{-1} = \sigma \sqrt{\frac{\pi}{2}} \left[\mathrm{erf}\left(\frac{(b_r - b_0)}{\sqrt{2}\,\sigma}\right) - \mathrm{erf}\left(\frac{(b_\ell - b_0)}{\sqrt{2}\,\sigma}\right)\right] \,, \tag{6}$$

where b_ℓ and b_r are the leftmost and rightmost points respectively of the domain of observation. In particular, the Gaussian least-squares fit to the data for each component

is computed allowing the mean and variance to vary freely while the amplitude is determined by Eq. (6).

The closeness of the PDF's of the perpendicular components of the magnetic field to Gaussian distributions is evident from Fig. 1 and from the value of χ^2 and the kurtoses listed in Table 1. Note that we define the kurtosis for the distribution of a specified component by

$$\kappa := \frac{\langle (b - b_0)^4 \rangle}{\sigma^4} , \tag{7}$$

where b_0 is the mean and σ is the standard deviation of the given component. For practical purposes the ensemble mean in Eq. (7) is the arithmetic mean of the kurtoses computed on each interval.

The kurtosis of the parallel component is approximately 4.2 which is higher than the value 3.0 expected for a Gaussian distribution, according to the definition Eq. (7), whereas the perpendicular components have kurtoses approximately 3.0 and 3.7 which are closer to the Gaussian value. This indicates that the PDF of the parallel component (and of the second perpendicular component) is more peaked than a Gaussian as evidenced in Fig. 1; however the kurtosis we compute is much closer to that of a Gaussian distribution than that obtained when the variation of the mean field is not taken into account [e. g. $\kappa \approx 11$, *Feynman and Ruzmaikin*, 1994]. Repeating the analysis without a stationarity test of the mean yields the kurtoses 3.0, 3.7, and 3.8. The first two values are unchanged, while the last is about 10% lower than the value obtained with the stationarity test. The stationarity test of the mean therefore does not bias our

data towards Gaussianity.

The mean field and variances computed on each interval are in turn not constant, and the spread is illustrated in Table 2 and Fig. 2. The plot shows the PDF of the mean field (mean value of parallel component). It is seen to have a single peak and resembles a saw-tooth distribution, however the uncertainty in the determination of the mean field is approximately 0.4 nT, as determined by Eq. (9), and is large enough to allow distributions other than saw-tooth to fit the data. The PDF's of the variances of the three components are shown in Fig. 6. These distributions approximate lognormal functions, and have a wide range of variability. This feature suggests the applicability of the Castaing formulation to model the PDF's of the magnetic field components, and is explored in Sec. 4.

Table 2

Fig. 2

Fig. 6

The plots shown in Fig. 3 are obtained from Ulysses 1 minute averaged data analyzed using 96 h intervals. The perpendicular component PDF's are very nearly Gaussian ($\kappa \approx 2.9$ in either case), while the parallel component has a somewhat higher value of the kurtosis ($\kappa \approx 4.1$) and a poorer Gaussian fit. Once again it is found that the stationarity test of the mean does not bias our data towards Gaussianity; the kurtoses values are 2.9, 3.0, and 3.4 when the analysis is repeated without the data selection procedure using the stationarity test.

Fig. 3

In the case of the Omnitape, the data spans 30 years, whereas the Ulysses data spans 2 months. This leads to poorer determination of the PDF's of the mean field and of variances. Under these circumstances, a non-representative fluctuation can cause noticable departures from Gaussianity such as those evident in the lower two panels of

Fig. 3.

Finally, the plots presented in Fig. 4 are obtained from analysis of the same Ulysses data as above, but the length of the interval of analysis is 24 h instead of the 96 h intervals used previously. The determination of the mean field is poorer than in the previous case due to the shorter length of the interval (see Eq. (9)), leading to greater errors in the PDF's of the fluctuations and of the mean field and variances. The kurtoses of the perpendicular components are approximately 3.2 and 2.3, while the parallel component once again shows higher kurtosis, approximately 6.0. (The values of the kurtoses without the use of a stationarity test of the mean are 2.8, 2.4, 4.7.) The plots illustrate the sensitivity to the length of the interval of analysis. Note that the kurtosis of the parallel component is almost 50% higher than that computed from the same data using 96 h intervals. This trend of larger departures from Gaussian distributions for shorter lengths of the interval of analysis parallels earlier results [*Marsch and Tu*, 1994; *Bruno et al.*, 1999] that show that the PDF's of increments are progressively more non-Gaussian at smaller values of the lag, but the precise relationship between the two analyses is not clear.

Fig. 4

3.1. Statistical Error Analysis

Determination of the mean field and other statistical parameters of the magnetic field fluctuations are subject to statistical errors. The finite-time estimation of the mean field,

$$[B]_T := \frac{1}{T}\int_0^T B(\tau)\, d\tau\,, \tag{8}$$

leads to the error, as given by classical ergodic theory [e. g. *Panchev*, 1971]

$$\Delta^2[B]_T = 2\,\sigma^2\,\frac{T_c}{T} + \mathcal{O}\left(\frac{T_c^2}{T^2}\right)\,, \tag{9}$$

where

$$\Delta^2[B]_T := \langle([B]_T - B_0)^2\rangle\,,$$

B_0 is the ensemble-averaged mean field, and $\langle\cdots\rangle$ denotes ensemble average. The correlation time T_c is defined by

$$T_c := \int_0^\infty \frac{R(\tau)}{R(0)} d\tau\,, \tag{10}$$

where $R(\tau)$ is the autocorrelation function, $\langle\delta B(t+\tau)\,\delta B(t)\rangle$, and $\delta B(t) := B(t) - B_0$.

There are two sources of error in the estimation of the variances. The first is due to systematic underestimation of the variance due to loss of low frequency power that results from finite-time-estimation. This is given by

$$\langle[\sigma^2]_T\rangle = \sigma^2 - \Delta^2[B]_T\,. \tag{11}$$

The second source of error is statistical and an estimate is found in a manner analogous to the estimate for error in the mean value obtained in Eq. (9). The result is expressed as

$$\Delta^2[\sigma^2]_T = 2\,(\kappa - 1)\,\sigma^4\,\frac{T_*}{T} + \mathcal{O}\left(\frac{T_*^2}{T^2}\right)\,, \tag{12}$$

where

$$\Delta^2[\sigma^2]_T := \langle([\sigma^2]_T - \sigma^2)^2\rangle - (\Delta^2[B]_T)^2$$

and

$$T_* := \int_0^\infty \frac{R^2(\tau)}{R^2(0)} d\tau\,. \tag{13}$$

In obtaining Eq. (12) an assumption of structural similarity of correlation functions is made [*Townsend*, 1976] which allows us to extend the relation

$$\langle \delta B^4 \rangle = \kappa \langle \delta B^2 \rangle^2 ,$$

(where κ is the kurtosis) to non-zero lags:

$$\langle \delta B^2(t)\, \delta B^2(t+\tau) \rangle = \langle \delta B^2(t) \rangle \langle \delta B^2(t+\tau) \rangle + (\kappa - 1) \langle \delta B(t)\, \delta B(t+\tau) \rangle^2 .$$

Another assumption made in obtaining Eqs. (9) and (12) is that the autocorrelation function $R(\tau)$ is of Lanczos-type, i. e. $R(\tau) \approx 0$ for large values of τ.

There is a third source of error due to the uncertainty in the direction of the mean field, but it is relatively small. Additionally, it does not cause an error in the sum of variances $\Sigma_i \sigma_i^2$ and affects only the individual variances. We therefore neglect this error here.

The expected error in the determination of the mean field as expressed by Eq. (9) provides a criterion to judge the stationarity of the statistical mean on an interval [*Matthaeus and Goldstein*, 1982]. A given interval is decomposed into a collection of all possible subintervals each of length T, and the quantity $\Delta^2[B]_T$ is computed for this "ensemble". We have chosen to reject all intervals for which $\Delta^2[B]_T$ deviates from the expected value $2\,\sigma^2\, T_c/T$ by more than 67%.

In the case of the Omnitape data analysis using 96 h intervals, the mean field strength is observed to be 3.6 nT. The uncertainty, as computed from Eq. (9) is 0.8 nT, whereas the standard deviation of the mean field distribution is 1.4 nT (see Table 2). Similarly, the mean values of the variances of each component and their standard

deviations as well as expected uncertainty from Eq. (12) are listed in Table 2. (Table 2 does not show the corresponding values for the Ulysses data since determination of the PDF's of the mean field and variances is much poorer than for the Omnitape data.) In each case it is noticed that the standard deviations of the distributions are much higher than the expected uncertainties from the ergodic theory calculations. This suggests that there is a genuine spread in the distributions of the mean field and variances in addition to the finite sampling uncertainty [*Bury*, 1999]. It seems reasonable that this additional variability represents factors, such as large scale gradients and nonsteady solar sources, that are not controlled locally.

3.2. Effect of Variations of the Mean Field

Separating the short-time-scale fluctuations of the magnetic field from the longer-time-scale variations of the mean field, presumably a property of the solar source, is an important feature of our analysis. Variability of the mean can artificially enhance estimates of non-Gaussianity. We illustrate this with an example.

Following *Feynman and Ruzmaikin* [1994] we analyze hourly averaged Omnitape data from 1973. Treating the entire data set as one interval, without separating the fluctuations from the mean field, we find that the kurtosis of the PDF of the second perpendicular component is 10.3. This is similar to the kurtosis (approximately 11) reported by *Feynman and Ruzmaikin* [1994] for the B_z component, which is one of the nonradial components in the GSE coordinates. On the other hand, when the same data set is analyzed using 96 hr subintervals to separate the mean field from the fluctuations,

the kurtosis for the PDF of the fluctuations of the second perpendicular component drops dramatically to 3.6. This is still higher than the value (3.0) expected for a Gaussian distribution, but clearly demonstrates that the departure from Gaussianity is much larger when the variation of the mean field is not separated out.

3.3. Differences among distributions in the fast and slow wind

Our analysis can be further refined by differentiating between intervals with fast and slow wind. From an analysis of 2 days of slow wind data and 4 days of fast wind data, *Marsch and Tu* [1994] conclude that PDF's of field increments in the slow wind are more non-Gaussian than those in the fast wind at all scales. Here we examine the differences between fast and slow wind in regard to distributions of the fluctuations about the mean. We study the same 30 year Omnitape data set as described above, and separate the 96 hr intervals with slow speed (below 475 km/s) from those with high speed (above 525 km/s). If an interval has less than 75% acceptable data points, it is rejected by the algorithm. The PDF's of magnetic field components in the fast and slow solar winds are compared in three distinct cases. In the first case, the PDF's of the magnetic field components are computed on all available fast and slow wind intervals over a period of 30 years. In the second case, the PDF's of the fast and slow wind intervals are computed over a period of 4 years near the solar cycle minimum of 1976, while in the third case, the period of 4 years is near the solar cycle maximum of 1981.

The kurtoses of the PDF's are listed in Table 3 and variances in Table 4 for each of the three cases. The PDF's of the second perpendicular component are illustrated in

Table 3

Table 4

Fig. 5. Note that the distributions in the fast and slow solar wind do not display striking differences. A trend that one does observe in the PDF's is that they are generally narrower in the fast wind than in the slow wind — the standard deviations differ by less than 10%. The departures from Gaussianity of PDF's in both the fast and slow wind are small and the difference in kurtoses is less than 3.5%. Measures of non-Gaussianity of the magnetic field in the fast and slow winds is thus likely to be the same. This similarity between fast and slow wind fluctuations contrasts the well known features which differ greatly between the two [*Axford and McKenzie*, 1997]. Fig. 5

4. Castaing superposition model

We now turn our attention to a theoretical model that is capable of reproducing the small departures from Gaussianity seen in the higher order even moments of the distributions. The model involves a simple superposition of Gaussian distributions with variances that are distributed lognormally. It was originally proposed by *Castaing et al.* [1990] in the context of hydrodynamic turbulence and has also been applied by *Sorriso-Valvo et al.* [1999] in relation to distributions of increments of the magnitude of the interplanetary magnetic field. In contrast, we adapt the Castaing superposition to model the PDF's of the fluctuations of the components and from them derive the PDF of the magnitude of the fluctuations. (Note that fluctuations and increments are not identical; the relationship between PDF's of the two quantities is not straightforward.) Our approach is also distinguished by the use of *observed* distributions of the variances whereas *Sorriso-Valvo et al.* [1999] determine the width of the lognormal distribution of

the variance of the magnitude from a fitting technique.

4.1. Components of fluctuations

Adapting the formulation of *Castaing et al.* [1990], the PDF of the fluctuations of the ith component is a weighted superposition of Gaussian distributions:

$$f_i(b_i) := \int w(v_i)\, g(b_i, v_i)\, dv_i \,, \tag{14}$$

where $g(b_i, v_i)$ is a Gaussian distribution of b_i with variance v_i,

$$g(b_i, v_i) := \frac{1}{\sqrt{2\,\pi\, v_i}} \exp\left(\frac{-b_i^2}{2\, v_i}\right) . \tag{15}$$

The weighting function $w(v_i)$ is a lognormal distribution of the variance,

$$w(v_i) = \frac{1}{\sqrt{2\,\pi}\lambda\; v_i} \exp\left(-\frac{(\ln \frac{v_i}{v_{i0}})^2}{2\,\lambda^2}\right) , \tag{16}$$

where λ and v_{i0} are parameters that determine the width and mean of the distribution. The function $w(v_i)$ represents the distribution of variances due to multiple sources contained in the dataset. The integration in Eq. (14) is carried out over the range of variances that is observed in the data set.

The parameters λ and v_{i0} are determined empirically by a best-fit lognormal curve to the observed distribution of the variances. Lognormal best-fits to the observed distributions of variances are shown in Fig. 6 and the Castaing-superposed PDF's are compared with the observations in Fig. 7. The χ^2 values, kurtoses, and sixth moments of the Castaing-superposed distributions compare well to the observed distributions, and are listed in Table 5. The normalized sixth moment m_6 of the distributions is defined

Fig. 7

Table 5

analogously to the kurtosis:

$$m_6 := \frac{\langle (b_i - b_{i0})^6 \rangle}{\sigma^6} \,. \tag{17}$$

The sixth moment contains additional information about the tails of the distributions. For a Gaussian distribution, $m_6 = 15$, and a higher value indicates that the tail of the distribution is more prominent. Even though the distribution functions are only subtly different to the eye, the Castaing superposition does a much better job than a Gaussian model does in accounting for the sixth moments of the observed distributions, as demonstrated in Table 5. Note that while the Castaing model yields better fits to components 2 and 3, it seems that component 1, which is one of the perpendicular components, is better described by a single Gaussian. The reason for this difference between the two perpendicular components is not clearly known at this time.

4.2. Magnitude of fluctuations

The PDF of the magnitude of the fluctuations is computed from the PDF's of the components (assumed independent) by integration of the product of the component distributions on the surface of a sphere [*Hartlep et al.,* 2000]:

$$f(b) = \int f_1(b_1)\, f_2(b_2)\, f_3(b_3)\, d\phi\, d\theta \,, \tag{18}$$

where $b_1 = b \sin\theta \cos\phi$, $b_2 = b \sin\theta \sin\phi$, and $b_3 = b \cos\theta$. When the Castaing superposition is used to determine the PDF's of the components, the PDF of the magnitude is given by

$$f(b) \;\; = \;\; \int g_1(b_1, v_1)\, g_2(b_2, v_2)\, g_3(b_3, v_3) \;\times$$

$$w_1(v_1)\, w_2(v_2)\, w_3(v_3)\, dv_1\, dv_2\, dv_3\, d\phi\, d\theta\,. \tag{19}$$

This model is compared to the observations in Fig. 8. For comparision, we also show the case in which $f(b)$ is computed assuming that the components have Gaussian distributions — given by the best-fit Gaussians to the component PDF's. Observe that the Castaing model yields $f(b)$ that agrees more closely with the observations. Fig. 8

The best-fit lognormal curve to the observed PDF of the magnitude of fluctuations is also shown in Fig. 8, and seen to be in excellent agreement although we are not aware of any theoretical justification for this similarity. Note that *Burlaga* [1991] studied the PDF of the magnitude of the total magnetic field, and not of the fluctuations. The total field magnitude distribution includes the distribution of the mean field, which is presumably a solar source effect. This difference between the two lognormal fits must be kept in mind.

5. Conclusions

We examine magnetic field data from the NSSDC Omnitape and Ulysses spacecraft to compute the PDF's of the components of the fluctuations and find that the distributions are much closer to being Gaussian when the variation of the mean field is taken into account. This is particularly true of the perpendicular components of the fluctuations. We arrive at this conclusion by inspecting the kurtoses of the PDF's and the χ^2 goodness-of-fit parameters. These parameters also provide quantitative measures of the small departures from Gaussianity.

The highest value of the kurtosis that we observe for fluctuations of the interplanetary magnetic field is 6.0 for the parallel fluctuations as seen from the Ulysses data. This value of the kurtosis reduces to 4.1 when the same data is analyzed using a longer (96 h) interval of analysis that is less prone to errors in computing the mean field. Another example of the sensitivity of the PDF's to the details of the analysis is presented in Sec. 3.2, where it is seen that the kurtoses of the PDF's with and without the removal of the varying mean field are sharply different. This may explain why *Feynman and Ruzmaikin* [1994] report large departures from Gaussianity in contrast to the conclusion of *Whang* [1977].

In a study of the differences of the PDF's in fast and slow solar wind in the ecliptic plane, we find that the distributions of both fast and slow wind fluctuations are systematically non-Gaussian, with the kurtoses of the vector components lying in the range of 2.8–4.8. No significant difference in kurtoses is seen between the fast and slow samples in the entire dataset or in either solar maximum or solar minimum subsets. This is a surprising and interesting conclusion in view of the many observed differences between high and low speed wind. Our conclusion supports the view of *Smith and Balogh* [1995] – that the distribution functions of magnetic fluctuations in the fast and slow wind in the ecliptic plane are nearly identical – and reinforces this view quantitatively. In contrast, *Marsch and Tu* [1994] concluded that fluctuations in the slow wind are more non-Gaussian than fluctuations in the fast wind, particularly on time scales of several hours. Our conclusion also supports the findings of *Sorriso-Valvo et al.* [1999], who study a certain power law exponent associated with the PDF of the

magnitude of the magnetic field, and conclude that the differences between fast and slow solar wind are not significant.

Our analysis indicates that the departures from Gaussianity are generally such that the kurtosis robustly assumes values $\kappa \approx 3$ to 4. A small but systematic departure from Gaussian statistics may signify a universal property of interplanetary MHD turbulence. From standard treatments of hydrodynamic turbulence such as the von Karman-Howarth equations [*Monin and Yaglom,* 1975, e. g.] we observe that a dynamical hierarchy exists in which the second order moments depend upon third order moments and so on. Spectral transfer and turbulent dissipation depend upon the existence of third order moments [*Proudman and Reid,* 1954] and can also be seen in the MHD Karman-Howarth equations [*Smith,* 1981]. For strictly Gaussian statistics of the velocity and magnetic fields, spectral transfer cannot occur because the third order moments vanish. Turbulence depends upon a small non-Gaussianity of the fluctuations. For the solar wind, which is presumably driven strongly near the sun and near stream interfaces, it would be reasonable to suppose that nonlinearity allows a relaxation towards Gaussianity in turbulent decay, while driving maintains a degree of non-Gaussianity. This picture would be consistent with a reproducible level of non-Gaussianity such as that which is consistent with the present observations.

Further detailed examination of the dynamical origins of non-Gaussianity of magnetic fluctuations would take us into the realm of multifractal scaling of higher order moments [*Burlaga,* 1991b], which is beyond the scope of the present paper. Although untested using our particular data analysis procedure, our present conclusions

may apply to the interplanetary velocity field fluctuations as well since a high degree of cross-correlation is often seen in the velocity and magnetic fields [*Belcher and Davis,* 1971].

Distinctive features of our data analysis include the use of the mean field coordinate system in which the component fluctuations are seen to be almost uncorrelated, use of a subinterval of analysis that allows us to distinguish between the mean field variation and fluctuations, and the use of a stationarity test of the mean as a data selection criterion. The PDF's of the mean field and of the variances of the three components are also presented to illustrate the spreads in these parameters that may arise due to variations in the solar sources. These distributions are wider than what is expected solely from finite sampling. Therefore we conclude that statistical distributions of the mean field and the variances are significant features of magnetic fluctuations in the solar wind. Furthermore, the PDF's of variances of the magnetic field fluctuations are approximately lognormal, suggesting the applicability of the superposition principle of *Castaing et al.* [1990] to model the PDF's of the components.

In essence, the Castaing model is a superposition of Gaussian distributions with variances that are distributed lognormally. Such a model is physically plausible since it is well known that the IMF at low latitudes arises from many discrete coronal sources. If it is postulated that each of these discrete sources gives rise to Gaussianly distributed magnetic field components, it follows from the multiplicity of the sources that one may expect a spread of variances in the net magnetic field fluctuations that arise from the sum of all sources. The distribution of the variances may be considered a property of the

sources and is a measure of the relative numbers of sources that give rise to magnetic field fluctuations with specific values of the variance.

The PDF's and their kurtoses that arise from the Castaing model agree well with the observations. Additionally, the model leads to better agreement with the observed PDF of the magnitude of the fluctuations than a model that derives the PDF of the magnitude assuming that the components have Gaussian distributions. It may be noted that for reasons that are not presently understood, the first of the two perpendicular components has an almost purely Gaussian distribution, while the Castaing superposition is a good model for the other two components.

Acknowledgments. This work was supported by NASA grants NAG5-6570, NAG5-1573, NAG5-3026, and NAG5-8134 to the Bartol Research Institute.

References

Armstrong, J., J. M. Cordes and B. J. Rickett, Density power spectrum in the local inter-stellar medium, *Nature*, *291*, 561, 1981.

Axford, W. I., and J. F. McKenzie, The solar wind, in *Cosmic Winds and the Heliosphere*, edited by J. R. Jokipii, C. P. Sonett, and M. S. Giampapa, The University of Arizona Press, Tucson, 1997.

Balogh, A., T. J. Beek, R. J. Forsyth, P. C. Hedgecock, R. J. Marquedant, E. J. Smith, D. J. Southwood, and B. T. Tsurutani, The magnetic field investigation on the Ulysses spacecraft: Instrumentation and preliminary scientific results, *Astronomy and Astrophysics Supplement Series*, *92*, 221–236, 1992.

Batchelor, G. K., *Theory of Homogeneous Turbulence*, Cambridge U. Press, New York, p. 177, 1982.

Belcher, J. W., and L. Davis, Large-amplitude Alfvén waves in the interplanetary medium II, *Journal of Geophysical Research*, *76*, 3534–3563, 1971.

Bevington, P. R., *Data Reduction and Error Analysis for the Physical Sciences*, McGraw-Hill, 1969.

Bruno, R., B. Bavassano, E. Pietropaolo, V. Carbone, and P. Veltri, Effects of intermittency on interplanetary velocity and magnetic field fluctuations anisotropy, *Geophysical Research Letters*, *26*, 3185–3188, 1999.

Burlaga, L. F., Intermittent turbulence in the solar wind, *Journal of Geophysical Research*, *96*, 5847, 1991a.

Burlaga, L. F., Multifractal structure of the interplanetary magnetic field, *Geophysical Research Letters*, *18*, 69, 1991b.

Burlaga, L. F., and J. H. King, Intense interplanetary magnetic fields observed by geocentric spacecraft during 1963–1975, *Journal of Geophysical Research*, *84*, 6633, 1979.

Burlaga, L. F., and N. F. Ness, Magnetic field strength distributions and spectra in the heliosphere and their significance for cosmic ray modulation: Voyager 1, 1980–1994, *Journal of Geophysical Research*, *103*, 29719–29732, 1998.

Bury, K., *Statistical Distributions in Engineering*, Cambridge University Press, 1999.

Castaing, B., Y. Gagne, and E. J. Hopfinger, Velocity probability density functions of high Reynolds number turbulence, *Physica D*, *46*, 177–200, 1990.

Feldman, W. C., and E. Marsch, Kinetic phenomena in the solar wind, in *Cosmic Winds and the Heliosphere*, edited by J. R. Jokipii, C. P. Sonett, and M. S. Giampapa, The University of Arizona Press, Tucson, 1997.

Feynman, J., and A. Ruzmaikin, Distributions of the interplanetary magnetic field revisited, *Journal of Geophysical Research*, *99*, 17645–17651, 1994.

Frisch, U., P. L. Sulem, and M. Nelkin, A simple dynamical model of intermittent fully developed turbulence, *J. Fluid Mech.*, *87*, 719, 1978.

Goldstein, B. and G. L. Siscoe, Spectra and cross spectra of solar wind parameters from Mariner 5. In *Solar Wind II*, eds. C. P. Sonnett, P. J. Coleman and J. M. Wilcox, NASA Spec. Publ., 506, 1972.

Goldstein, B. E., E. J. Smith, A. Balogh, T. S. Horbury, M. L. Goldstein, and D. A. Roberts,

Properties of magnetohydrodynamic turbulence in the solar wind as observed by Ulysses at high heliographic latitude, *Geophys. Res. Lett.*, *22*, 3393–3396, 1995.

Grappin, R., A. Pouquet, and J. Léorat, Dependence of MHD turbulence spectra on the velocity field-magnetic field correlation, *Astron. Astrophys.*, *126*, 51, 1983.

Hartlep, T., W. H. Matthaeus, N. S. Padhye, C. W. Smith, Magnetic field strength distribution in interplanetary turbulence, *Journal of Geophysical Research*, *105*, 5135–5139, 2000.

Heisenburg, W., Zur statistichen theorie der turbulenz, *Z. Physik*, *124*, 628, 1948.

Hundhausen, A. J., *Solar Wind and Coronal Expansion*, Physics and Chemistry in Space Vol. 5, edited by J. G. Roederer, Springer-Verlag, New York, 1972.

Kabin, K., and V. O. Papitashvili, Fractal properties of the interplanetary magnetic field and the Earth's magnetotail field, *Earth Planets Space*, *50*, 87–90, 1998.

King, J. H., and N. E. Papitashvili, Interplanetary Medium Data Book — Supplement 5, 1988–1993, (Rep. NSSDC/WDC-A-R&S 94–08, NASA, Greenbelt, MD), 1994.

Lesieur, M., *Turbulence in Fluids*, Nijhoff, Dordrecht, The Netherlands, 1990.

Marsch, E., and C. Y. Tu, Non-Gaussian probability distributions of solar wind fluctuations, *Annales Geophysicae*, *12*, 1127, 1994.

Marsch, E., C. Y. Tu, and H. Rosenbauer Multifractal scaling of the kinetic energy flux in solar wind turbulence *Annales Geophysicae*, *14*, 259, 1996.

Matthaeus, W. H., and C. W. Smith, Structure of correlation tensors in homogeneous anisotropic turbulence, *Physical Review*, *A24*, 2135–2144, 1981.

Matthaeus, W. H., and M. L. Goldstein, Stationarity of MHD fluctuations in the solar wind, *Journal of Geophysical Research*, *87*, 10347, 1982.

Matthaeus, W. H., and M. L. Goldstein, Low-frequency 1/f noise in the interplanetary magnetic field, *Physics Review Letters*, *57*, 495–498, 1986.

Matthaeus, W. H., M. L. Goldstein, and J. H. King An interplanetary magnetic field ensemble at 1 AU, *Journal of Geophysical Research*, *91*, 59, 1986.

Millionshchikov, M. D., *Theory of homogeneous isotropic turbulence*, Dokl. Akad. Nauk SSSR *32*, 611, 1941.

Monin, A.S. and Yaglom, A.M., *Statistical Fluid Mechanics*, MIT Press, Cambridge, Mass., 1975.

Montgomery, D. C., M. R. Brown,and W. H. Matthaeus, Density Fluctuation Spectra in MHD Turbulence, *J. Geophys. Res.*, *92*, 282, 1987.

Mullan, D. J., Sources of the solar wind: What are the smallest-scale structures?, *Astronomy and Astrophysics*, *232*, 520, 1990.

Orszag, S. A., Analytical theories of turbulence, *J. Fluid Mech.*, *363*, *41*, 1970.

Panchev, S., *Random Functions and Turbulence*, Pergamon Press, 1971.

Phillips, J. L., S. J. Bame, A. Barnes, B. L. Barraclough, W. C. Feldman, B. E. Goldstein, J. T. Gosling, G. W. Hoogeveen, D. J. McComas, M. Neugebauer and S. T. Suess, Ulysses solar wind plasma observations from pole to pole, *Geophys. Res. Lett.*, *22*, 3301–3304, 1995.

Politano, H., and A. Pouquet, Model of intermittency in magnetohydrodynamic turbulence, *Phys. Rev. E*, *52*, 636–641, 1995.

Proudman, I., and W. H. Reid, On the decay of a normally distributed and homogeneous turbulent velocity field, *Phil. Trans. Roy. Soc. A*, *247*, 926, 1954.

Ruzmaikin, A., J. Feynman, B. E. Goldstein, E. J. Smith, and A. Balogh, Intermittent turbulence in solar wind from the south polar hole, *Journal of Geophysical Research*, *100*, 3395–3403, 1995.

She, Z. S., and E. Leveque Universal scaling laws in fully-developed turbulence, *Phys. Rev. Lett.*, *72*, 336–339, 1994.

Slavin, J. A., and E. J. Smith, Solar cycle variations in the interplanetary magnetic field, in Solar Wind Five, *NASA Conf. Pub.*, *2280*, 323–331, 1983.

Smith, C. W., *The Structure of Axisymmetric Turbulence*, Ph.D. Thesis, College of William and Mary, Williamsburg, Virginia, 1981.

Smith, E. J., and A. Balogh, Ulysses observations of the radial magnetic field, *Geophys. Res. Lett.*, *22*, 3317-3320, 1995.

Smith, E. J., and R. G. Marsden, Ulysses observations from pole-to-pole: Introduction, *Geophysical Research Letters*, *22*, 3297–3300, 1995.

Sorriso-Valvo, L., V. Carbone, P. Veltri, G. Consolini, and R. Bruno, Intermittency in the solar wind turbulence through probability distribution functions of fluctuations, *Geophysical Research Letters*, *26*, 1801–1804, 1999.

Townsend, A. A., *The Structure of Turbulent Shear Flow*, Cambridge University Press, 1976.

Tu, C. Y., and E. Marsch, MHD structures, waves and turbulence in the solar wind – observations and theories, *Space Science Rev.*, *73*, 1–210, 1995.

Wang, L. P., S. Y. Chen, and J. G. Brasseur, Examination of hypotheses in the Kolmogorov

refined turbulence theory through high-resolution simulations. Part 2. Passive scalar field, *J. Fluid Mech.*, *400*, 163–197, 1999.

Whang, Y. C., Probability distribution function of mesoscale magnetic fluctuations during quiet conditions, *Solar Physics*, *53*, 507–517, 1977.

Zank, G. P. and Matthaeus, W. H., Nearly Incompressible Fluids. II: Magnetohydrodynamics, Turbulence, and Waves, *Phys. Fluids A*, *5*, 257, 1993.

N. S. Padhye, C. W. Smith, and W. H. Matthaeus, Bartol Research Institute, University of Delaware, Newark, DE 19716.

(e-mail: [nikhil, chuck, yswhm]@bartol.udel.edu)

Received _____

Submitted to *Journal of Geophysical Research* (Space Physics): November 1999.

Figure 1. PDF's of fluctuations of the magnetic field as computed from Omnitape data analyzed using 96 h intervals. The top two plots show the perpendicular components, while the bottom one shows the parallel component. The dots represent centers of the binned data and the solid line shows the best-fit Gaussian. Each of the 50 bins contains 3167 measurements. The uncertainty in the abscissas of the bins is uniformly less than 0.5% of the bin widths.

Figure 2. The plot shows the PDF of the mean magnetic field B_0 computed from Omnitape data analyzed using 96 h intervals. Each of the 11 bins contains 164 data points. The uncertainty in the abscissas of the bins is uniformly less than 2.5% of the bin widths.

Figure 3. PDF's of fluctuations of the magnetic field as computed from Ulysses data analyzed using 96 h intervals. The top two plots show the perpendicular components, while the bottom one shows the parallel component. The dots represent centers of the binned data and the solid line shows the best-fit Gaussian. Each of the 50 bins contains 5034 measurements. The uncertainty in the abscissas of the bins is uniformly less than 0.5% of the bin widths.

Figure 4. PDF's of fluctuations of the magnetic field as computed from Ulysses data analyzed using 24 h intervals. The top two plots show the perpendicular components, while the bottom one shows the parallel component. The dots represent centers of the binned data and the solid line shows the best-fit Gaussian. Each of the 50 bins contains 2876 measurements. The uncertainty in the abscissas of the bins is uniformly less than 0.5% of the bin widths.

Figure 5. PDF's of the second perpendicular component in fast (dots) and slow (pluses) solar wind. The corresponding best-fit Gaussians are also shown alongside. From top to bottom, plots represent observations from the entire ensemble, during a 4 year period near the solar cycle minimum of 1976, and during a 4 year period near the solar cycle maximum of 1981 respectively.

Figure 6. Observed PDF's (dots) of the variances of the components of the magnetic field and the best-fit lognormal curves (solid lines). The top two plots are for the perpendicular components and the bottom one is for the parallel component. The widths of the lognormal curves are $\lambda = 0.52$, 0.72, and 0.89 respectively.

Figure 7. Observed PDF's (dots) of the fluctuations of the components of the magnetic field, the Castaing-superposed PDF's (solid lines), and the best-fit Gaussian curves (dashed lines). The top two plots are for the perpendicular components and the bottom one is for the parallel component.

Figure 8. Observed PDF's (dots) of the magnitude of magnetic field fluctuations, the PDF computed from the Castaing-superposed PDF's of the components (solid line), the PDF computed from the best-fit Gaussian PDF's of the components (dashed line), and the best-fit lognormal curve (dash-dotted line).

Figure 1. PDF's of fluctuations of the magnetic field as computed from Omnitape data analyzed using 96 h intervals. The first two plots show the perpendicular components, while the last one shows the parallel component. The dots represent centers of the binned data and the solid line shows the best-fit Gaussian. Each of the 50 bins contains 3167 measurements. The uncertainty in the abscissas of the bins is uniformly less than 0.5% of the bin widths.

Figure 2. The two plots show the PDF's of the mean magnetic field B_0 and of the sum of variances, denoted σ^2, of the three components, as computed from Omnitape data analyzed using 96 h intervals. Each of the 11 bins contains 164 data points. The uncertainty in the abscissas of the bins is uniformly less than 2.5% of the bin widths.

Figure 3. PDF's of fluctuations of the magnetic field as computed from Ulysses data analyzed using 96 h intervals. The first two plots show the perpendicular components, while the last one shows the parallel component. The dots represent centers of the binned data and the solid line shows the best-fit Gaussian. Each of the 50 bins contains 5034 measurements. The uncertainty in the abscissas of the bins is uniformly less than 0.5% of the bin widths.

Figure 4. PDF's of fluctuations of the magnetic field as computed from Ulysses data analyzed using 24 h intervals. The first two plots show the perpendicular components, while the last one shows the parallel component. The dots represent centers of the binned data and the solid line shows the best-fit Gaussian. Each of the 50 bins contains 2876 measurements. The uncertainty in the abscissas of the bins is uniformly less than 0.5% of the bin widths.

Figure 5. PDF's of the second perpendicular component in fast (dots) and slow (pluses) solar wind. The corresponding best-fit Gaussians are also shown alongside. From top to bottom, plots represent observations from the entire ensemble, during a 4 year period near the solar cycle minimum of 1976, and during a 4 year period near the solar cycle maximum of 1981 respectively.

Figure 6. Observed PDF's (dots) of the variances of the components of the magnetic field and the best-fit lognormal curves (solid lines). The top two plots are for the perpendicular components and the bottom one is for the parallel component. The widths of the lognormal curves are $\lambda = 0.52$, 0.72, and 0.89 respectively.

Figure 7. Observed PDF's (dots) of the fluctuations of the components of the magnetic field, the Castaing-superposed PDF's (solid lines), and the best-fit Gaussian curves (dashed lines). The top two plots are for the perpendicular components and the bottom one is for the parallel component.

Figure 8. Observed PDF's (dots) of the magnitude of magnetic field fluctuations, the PDF computed from the Castaing-superposed PDF's of the components (solid line), the PDF computed from the best-fit Gaussian PDF's of the components (dashed line), and the best-fit lognormal curve (dash-dotted line).

Table 1. Kurtoses and χ^2 values

	Perp. 1	Perp. 2	Parallel
Omnitape 96h: Best-fit χ^2	0.0003	0.0075	0.0168
Kurtosis	2.99 ± 0.04	3.67 ± 0.05	4.17 ± 0.08
Ulysses 96h: Best-fit χ^2	0.0017	0.0058	0.0345
Kurtosis	2.95 ± 0.11	2.89 ± 0.16	4.10 ± 0.27
Ulysses 24h: Best-fit χ^2	0.0050	0.0068	0.0727
Kurtosis	3.18 ± 0.08	2.32 ± 0.05	5.98 ± 0.38

Table 2. Variability of the mean magnetic field and of the variances listed here is for Omnitape data using 96 h intervals for analysis. The rightmost column shows the uncertainties expected from the ergodic theory formulae specified in Sec. 3.1. The units are nT for the mean field, and $(\mathrm{nT})^2$ for the variances.

	Mean Value	Standard Deviation	Calculated Uncertainty
Mean Magnetic Field	3.6	1.4	0.8
Perp. Variance (First)	8.1	7.9	2.0
Perp. Variance (Second)	9.3	10.6	2.5
Parallel Variance	9.4	11.1	3.2

Table 3. Kurtoses in Fast and Slow Wind

Data set	Speed	$\kappa_{\perp 1}$	$\kappa_{\perp 2}$	$\kappa_{\parallel}$
Full Omnitape	Slow	2.9 ± 0.1	3.4 ± 0.1	4.2 ± 0.2
	Fast	2.9 ± 0.1	3.5 ± 0.2	4.5 ± 0.2
Solar Min. 1976	Slow	2.8 ± 0.1	3.4 ± 0.1	4.1 ± 0.3
	Fast	3.0 ± 0.1	3.2 ± 0.1	4.8 ± 0.3
Solar Max. 1981	Slow	3.0 ± 0.1	3.4 ± 0.1	4.3 ± 0.1
	Fast	3.3 ± 0.6	3.7 ± 0.5	3.9 ± 0.5

Table 4. Variances in Fast and Slow Wind

Data set	Speed	$\sigma^2_{\perp 1}$	$\sigma^2_{\perp 2}$	$\sigma^2_{\parallel}$
Full Omnitape	Slow	7.5	9.4	9.3
	Fast	5.1	5.7	4.6
Solar Min. 1976	Slow	5.9	6.4	7.5
	Fast	4.5	4.0	3.6
Solar Max. 1981	Slow	8.1	11.4	10.4
	Fast	8.2	8.8	7.2

Table 5. Comparision of the goodness-of-fit measure χ^2 and statistical properties, kurtoses and the normalized sixth moment m_6, of the Gaussian and Castaing models with the observations.

	Perp. 1	Perp. 2	Parallel
Gaussian best-fit χ^2	0.0005	0.0075	0.0230
Castaing best-fit χ^2	0.0080	0.0029	0.0116
Observed Kurtosis	3.0	3.7	4.2
Kurtosis for Gaussian Model	3.0	3.0	3.0
Kurtosis for Castaing Model	3.4	4.1	4.4
Observed m_6	16.4	27.4	41.0
m_6 for Gaussian Model	15.0	15.0	15.0
m_6 for Castaing Model	18.8	29.9	35.4

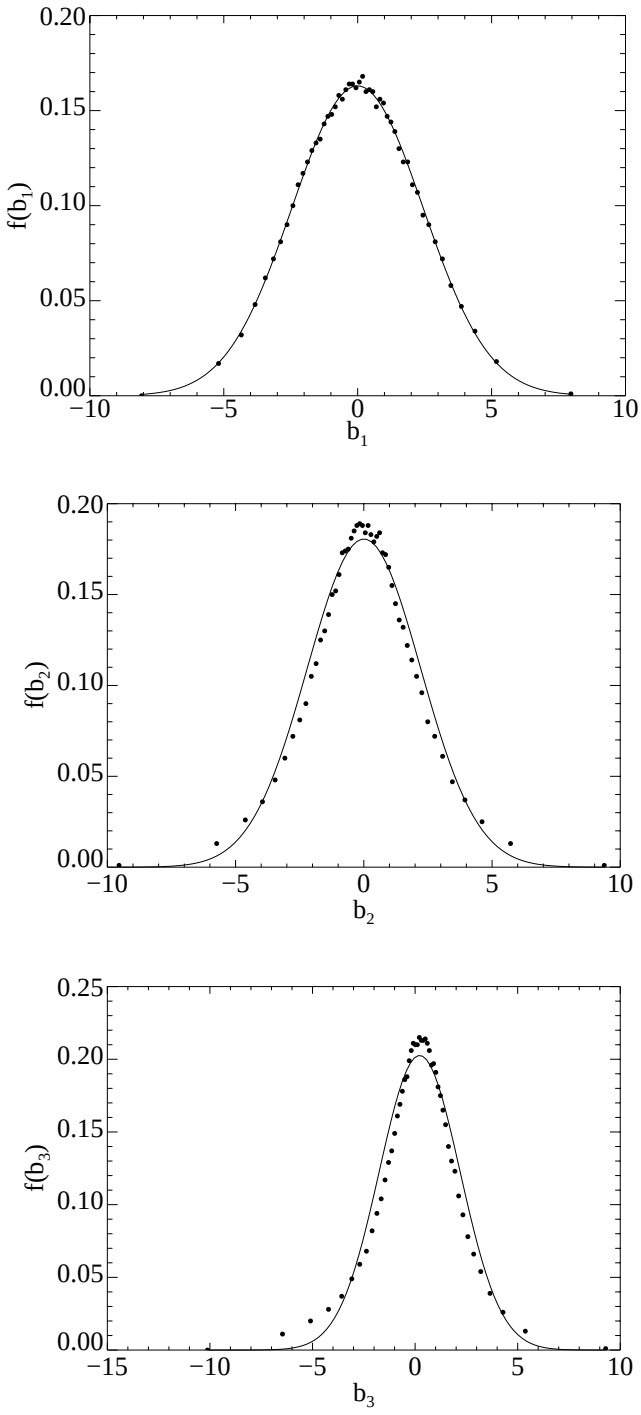
0.20
0.15
0.10
0.05
0.00
f(b1)
−10
−5
0
5
10
b1
0.20
0.15
0.10
0.05
0.00
f(b2)
−10
−5
0
5
10
b2
0.25
0.20
0.15
0.10
0.05
0.00
f(b3)
−15
−10
−5
0
5
10
b3

Figure 1.

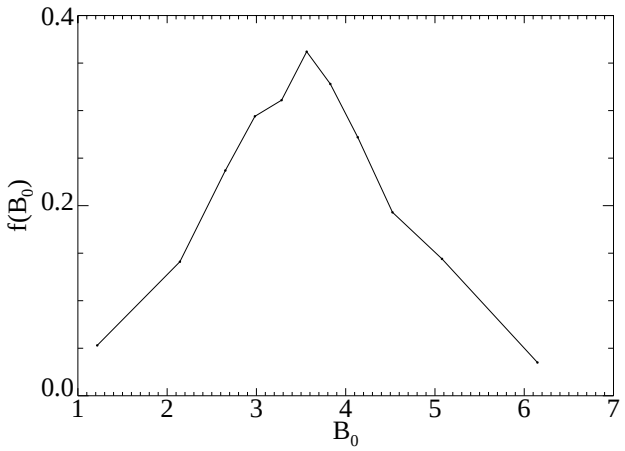

Figure 2.

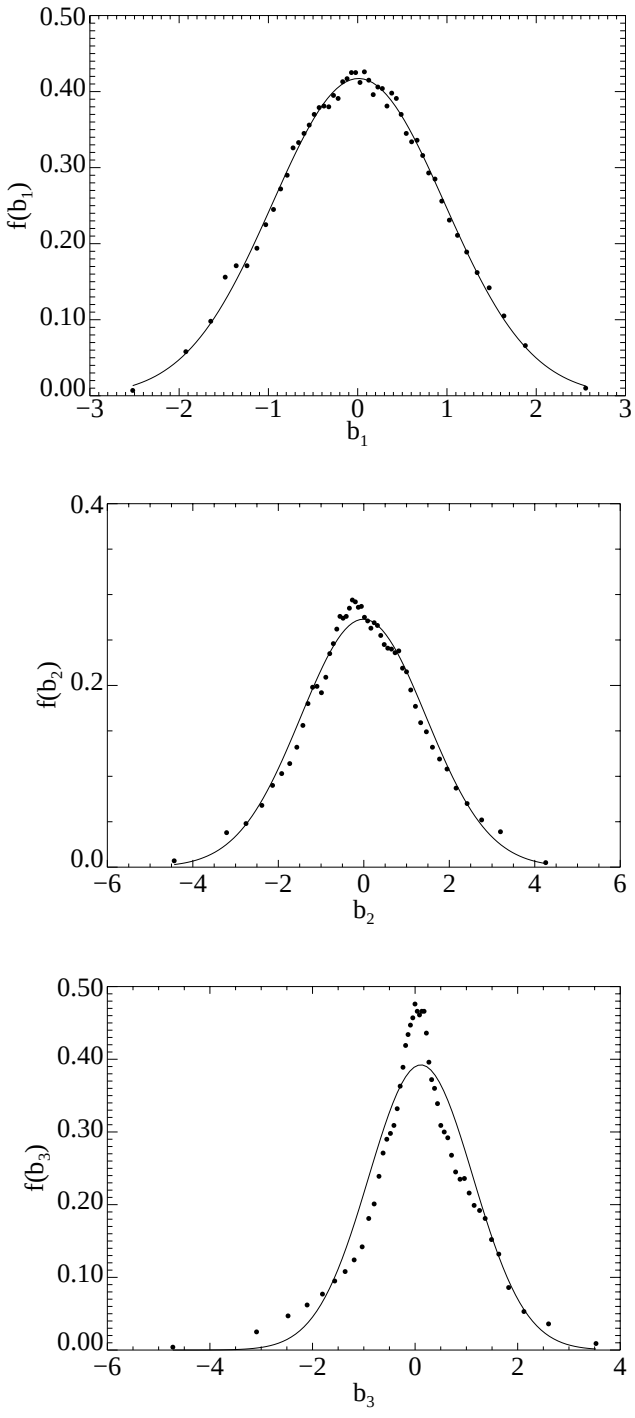
0.50
0.40
0.30
0.20
0.10
0.00
f(b1)
−3
−2
−1
0
1
2
3
b1
0.4
0.2
0.0
f(b2)
−6
−4
−2
0
2
4
6
b2
0.50
0.40
0.30
0.20
0.10
0.00
f(b3)
−6
−4
−2
0
2
4
b3

Figure 3.

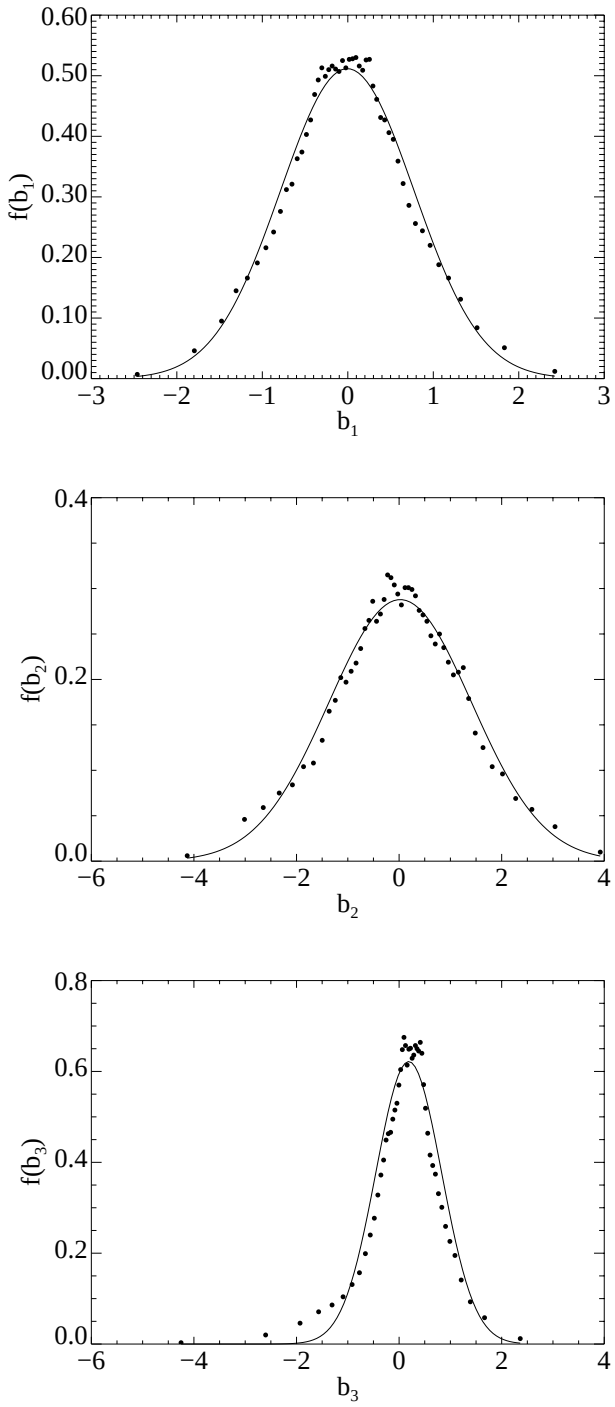
0.60
0.50
0.40
0.30
0.20
0.10
0.00
f(b1)
−3
−2
−1
0
1
2
3
b1
0.4
0.2
0.0
f(b2)
−6
−4
−2
0
2
4
b2
0.8
0.6
0.4
0.2
0.0
f(b3)
−6
−4
−2
0
2
4
b3

Figure 4.

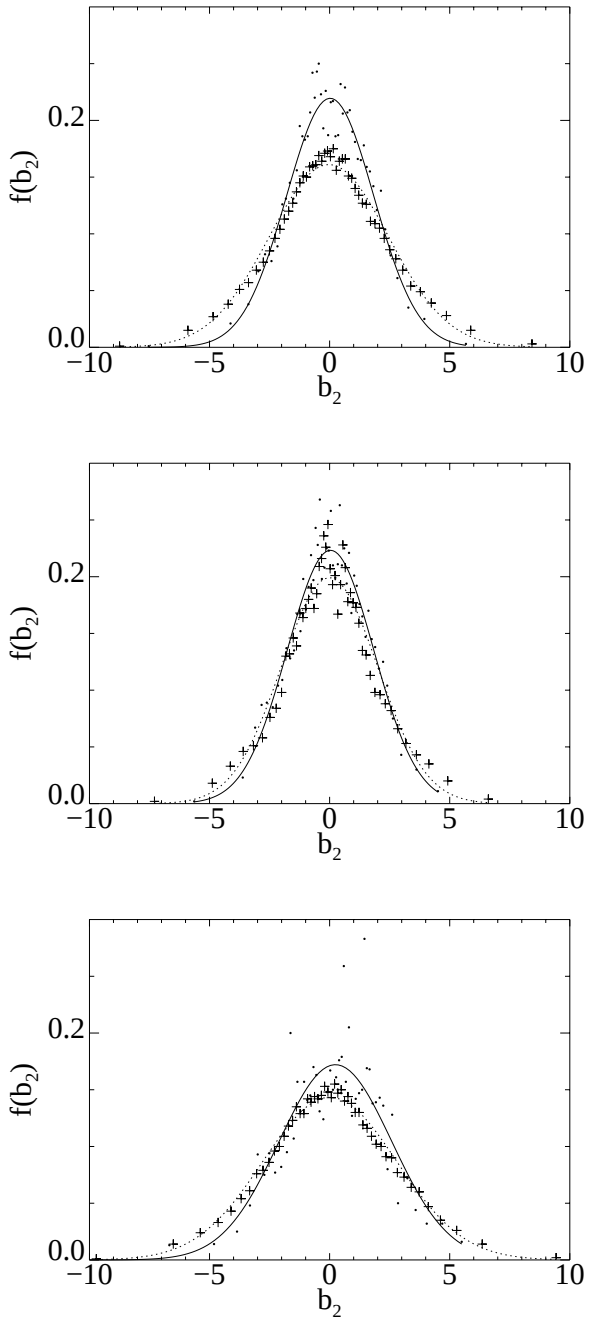

Figure 5.

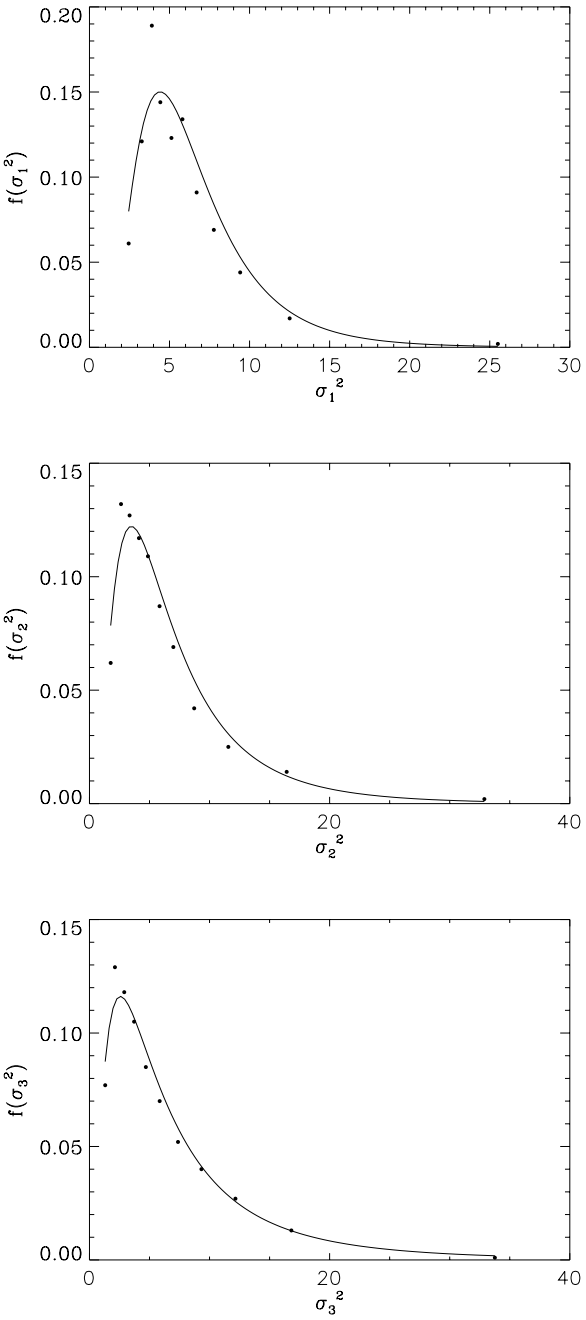
0.20
0.15
0.10
0.05
0.00
f(σ_1^2)
0
5
10
15
20
25
30
σ_1^2
0.15
0.10
0.05
0.00
f(σ_2^2)
0
20
40
σ_2^2
0.15
0.10
0.05
0.00
f(σ_3^2)
0
20
40
σ_3^2

Figure 6.

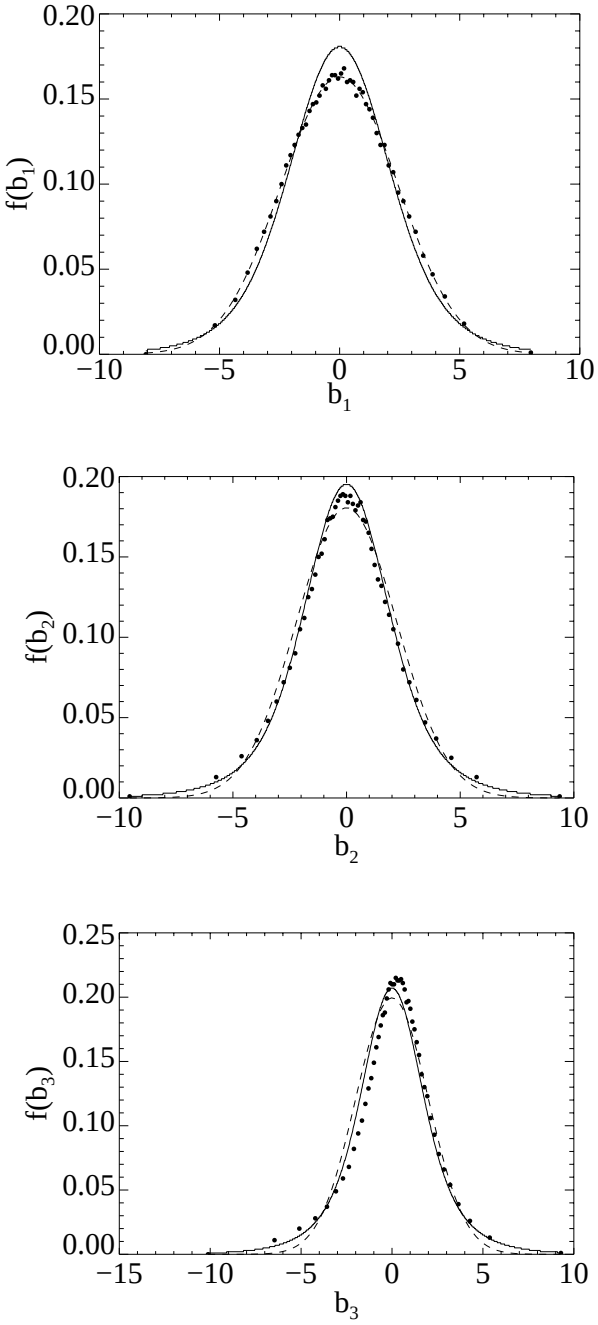
0.20
0.15
0.10
0.05
0.00
f(b1)
−10
−5
0
5
10
b1
0.20
0.15
0.10
0.05
0.00
f(b2)
−10
−5
0
5
10
b2
0.25
0.20
0.15
0.10
0.05
0.00
f(b3)
−15
−10
−5
0
5
10
b3

Figure 7.

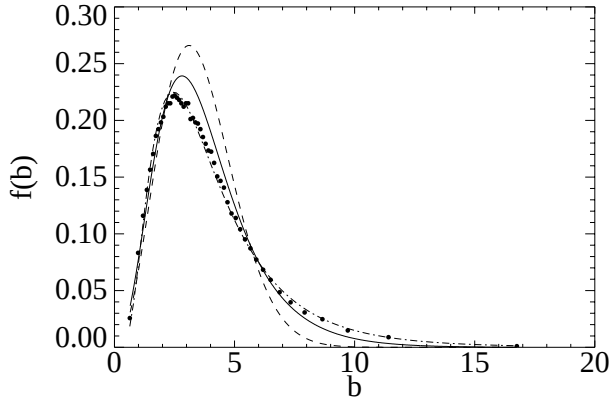

Figure 8.